PCCP

ROYAL SOCIETY OF CHEMISTRY

PAPER

View Article Online
View Journal | View Issue

Cite this: *Phys. Chem. Chem. Phys.*, 2021, **23**, 10835

Polarization-resolved single-molecule tracking reveals strange dynamics of fluorescent tracers through a deep rubbery polymer network†

Jaladhar Mahato, Sukanya Bhattacharya, Dharmendar K. Sharma ‡ and Arindam Chowdhury *

Received 10th November 2020,
Accepted 8th April 2021

DOI: 10.1039/d0cp05864e

rsc.li/pccp

Tracking the movement of fluorescent single-molecule (SM) tracers has provided several new insights into the local structure and dynamics in complex environments such as soft materials and biological systems. However, SM tracking (SMT) remains unreliable at molecular length scales, as the localization error (LE) of SM trajectories (~30–50 nm) is considerably larger than the size of molecular tracers (~1–2 nm). Thus, instances of tracer (im)mobility in heterogeneous media, which provide indicators for underlying anomalous-transport mechanisms, remain obscured within the realms of SMT. Since the translation of passive tracers in an isotropic media is associated with fast dipolar rotation, we propose that authentic pauses within the LE can be revealed by probing the hindrance of SM reorientational dynamics. Here, we demonstrate how polarization-resolved SMT (PR-SMT) can provide emission anisotropy at each super-localized position, thereby revealing the tumbling propensity of SMs during random walks. For rhodamine 6G tracers undergoing heterogeneous transport in a hydrated polyvinylpyrrolidone (PVP) network, analysis of PR-SMT trajectories enabled us to discern instances of genuine immobility and localized motion within the LE. Our investigations on 100 SMs in (plasticized) PVP films reveal a wide distribution of dwell times and pause frequencies, demonstrating that most probes intermittently experience complete translational and rotational immobilization. This indicates that tracers serendipitously encounter compact, rigid polymer cavities during transport, implying the existence of nanoscale glass-like domains sparsely distributed in a predominantly deep-rubbery polymer network far above the glass transition.

1. Introduction

The diffusion dynamics of single molecules (SMs) and fluorescent tracers have provided several new insights into local environments in complex systems such as bio-membranes,[1–3] cellular media,[4–6] as well as gel and polymer networks.[7–9] SM tracking (SMT) has emerged as one of the primary tools to probe transport processes in systems far from equilibrium.[10,11] In contrast to the Fickian diffusion observed in isotropic media, spatiotemporally inhomogeneous systems often exhibit anomalous transport.[12–14] For instance, during infection, individual virus particles within host cell's cytoplasm undergo localized and hindered diffusion apart from active transport.[15] Even for passive media such as polymer gel networks and solid–liquid interfaces, SM tracers have shown to exhibit both confined and subdiffusive motion.[9,16,17] Anomalous diffusion can have various origins,[18] such as obstructed diffusion,[19] fractional Brownian motion[8] and continuous-time random walk (CTRW).[17,20] In contrast to the former two, which arise from molecular crowding and memory effects, respectively, CTRW is characterized by intermittent pauses due to the tracers' association with components in the medium.[17,20] While the coexistence of multiple mechanisms can lead to subdiffusion,[21,22] the "stop and go" movement of tracers is frequently encountered in various biological systems both *in vivo*[21] and *in vitro*.[23] However, such momentary stops during transport can evade detection if their timescales or length scales are beyond the spatiotemporal resolution of SMT.

The localization precision in super-resolved imaging is the uncertainty in locating the exact position of a tracer, referred to as the localization error (LE), which depends on the number of detected photons.[24–26] Indeed, use of high laser excitation powers in super-localization methods allows for the determination of tethered single-emitters' locations down to sub-10 nanometers.[27,28] However, investigation of SM transport over several

Department of Chemistry, Indian Institute of Technology Bombay, Powai, Mumbai 400076, India. E-mail: arindam@chem.iitb.ac.in

† Electronic supplementary information (ESI) available. See DOI: 10.1039/d0cp05864e

‡ Present address: Department of Chemistry, Maulana Azad National Institute of Technology, Bhopal, 462003, India.

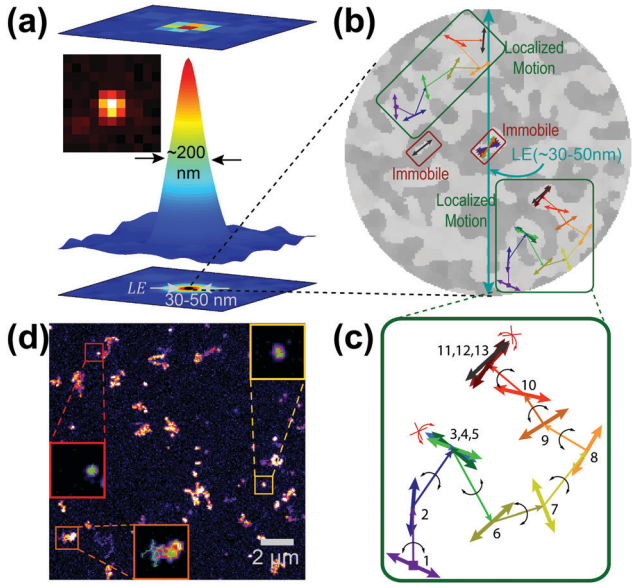

Fig. 1 Transport within localization error (LE). (a) Super-localization of a diffraction-limited spot, showing the typical dimensions of LE (bottom projection). (b) Schematic depiction of tracer navigation within the LE depicting possibilities of both immobility and localized motion. (c) Random walk of a single dipole with intermittent pauses. Arrows represent the whole molecule reorientation and numbers represent consecutive time points in the trajectory. (d) Maximum intensity projection (from 200 frames of a movie) of Rh6G probe in hydrated PVP polymer thin films (ambient RH ~75%) showing a wide range of translational motion ranging from confined to mobile tracers. Insets are magnifications of 1 μm^2 areas overlaid with super-resolved trajectories (see Fig. S1, ESI†).

seconds requires lowering the excitation power to minimize photo-bleaching/-blinking.[7,21,29] Besides, localization of rotationally immobile emitters often leads to an increase in LE, which may further augment for probes slightly away from the focal plane.[30–33] As a consequence, the LE of a super-resolved SM trajectory in a complex environment becomes at least a few tens of nanometers (Fig. 1a).[17,29,34,35] In spite of this uncertainty, when the determined position of a tracer remains within LE (~30–50 nm) over successive frames, it is often inferred that the probe remains in stasis.[8,9,17,21,29,34,35] However, the dimensions of LE are at least an order of magnitude larger than those of a molecular tracer (~1–2 nm), which implies that the emitter can be either static or translationally active over several nanometers (Fig. 1b). Consequently, there may be ambiguity in identifying translational movement or pauses within LE using SMT, altering the distribution of wait times which are relevant to infer the plausible tracer navigation mechanisms.[17,21,23,36] Thus, to unveil complexities during the transport processes of SMs in heterogeneous media, it is crucial to obtain authentic information on pauses in each a super-localized trajectory.

This motivated us to search for alternate approaches that can provide strong evidence for translational immobility of molecular tracers within the LE. In the condensed phase, molecules undergo very fast reorientation during translational diffusion, owing to large differences in their timescales.[37,38] Even in a highly viscous medium where the diffusivities (D_μ) of molecular tracers are low ($\sim 10^{-1}$ μm^2 s^{-1}), each measurable step during random walk is associated with a large number of tumbling events.[34,38,39] Therefore, identification of instances where a tracer is rotationally immobile would serve as an unambiguous indicator of stasis (Fig. 1c). Polarization-resolved SM fluorescence imaging has been extensively used to investigate slow timescale (<1 kHz) dipolar rotational dynamics in a variety of environments;[32,39–45] however, it has rarely been effectively coupled with SMT.[46,47] Here we show that simultaneous measurement of emission anisotropy and super-localized positions of SMs allows for the correlation of angular and positional displacements, which together portray intricate details of molecular navigation in heterogeneous soft materials.

As a case study, we investigated the transport of single rhodamine 6G (Rh6G) molecules in a plasticized (rubbery) polyvinylpyrrolidone (PVP) film, in which tracers undergo diverse diffusion dynamics ranging from confined motion, subdiffusion (majority) and normal diffusion.[48] The hydrated polymer matrix offers a heterogeneous viscoelastic network where SMs exhibit a wide range of translational characteristics (Fig. 1d and Fig. S1, ESI†). We have developed and subsequently utilized polarization-resolved single molecule tracking (PR-SMT) to discriminate between genuine stops and locally mobile events in each trajectory. Our analyses of PR-SMT data on 100 Rh6G molecules reveal the frequent occurrence of authentic pauses attributed to the intermittent association of SMs with extremely compact and rigid nanoscale cavities. This has intriguing implications in terms of the molecular scale morphology and dynamics of deep-rubbery polymer matrices.

2. Polarization-resolved single-molecule tracking

Our conceptualization of PR-SMT relies on the fast tumbling of a non-spherical passive tracer during its translational motion in an isotropic media in the absence of any external forces.[34,37,39] Even in extremely dense matrices, where molecular tracers (size ~ 1 nm) undergo extremely slow transport ($D_\mu \sim 10^{-4}$ μm^2 s^{-1}), the rotational correlation times (τ_R) have been shown to range from tens to hundreds of microseconds.[38] Further, τ_R exceeds milliseconds only for SMs embedded in polymer film matrices slightly above the glass transition temperature (T_g), where they are unable to translate beyond the dimensions of the polymer cavities. Therefore, in quasi-isotropic viscous media, the detection of individual dipoles for which tumbling is effectively arrested or severely hindered (τ_R ~ 50–500 ms) serves as an unambiguous indicator for translational immobility. Conversely, if the dipolar reorientation is relatively fast, it is unlikely that the tracer is tightly associated or confined in a compact nanodomain, implying that the tracer undergoes localized motion beyond a few nanometers within the LE.

Widefield fluorescence anisotropy imaging is ideally suited to investigate dipolar tumbling dynamics in highly viscous environments as it allows the detection of several SMs in each frame of a movie. Moreover, the emission polarization of each SM can be detected at timescales similar to that of SMT

(τ_{exp} ~ 10–30 Hz). While emission polarization is generally measured for translationally static dipoles, anisotropy imaging has also been utilized to probe the wobbling dynamics of SMs during 1-D transport.[46,47,49] Thus, determination of the super-localized positions and reorientational characteristics of mobile SMs in each frame of a movie can be realized *via* PR-SMT. To avoid artifacts arising from the fluorescence intermittency of SMs,[39,46] it is necessary to perform PR imaging by simultaneous measurement of intensities *via* two orthogonally polarized emission channels, $\{(I_s(t),I_p(t))\}$. Quantification of emission anisotropy is achieved by evaluation of linear dichroism (LD) trajectories, $LD(t) = \{I_s(t) - I_p(t)\}/\{I_s(t) + I_p(t)\}$.[50] A fixed orientation of a probe molecule most often leads to a non-zero LD(t) with nominal fluctuations, while slow-timescale dipolar reorientation is characterized by large-amplitude temporal modulation of LD(t). In contrast, fast reorientation of dipoles yields a zero-centered, narrow unimodal distribution (P(LD)) owing to temporal averaging of the intensity detected *via* the S-/P-channels, which can be easily distinguished from a P(LD) arising from hindered tumbling.[39] It is relevant to note that fast-rotating dipoles can be discriminated from immobile dipoles at equiangular orientation with respect to the S-/P-channels *via* rotation of the analyzer by ±45°; P(LD) remains unaffected in the former situation, while for fixed dipoles P(LD) is no longer zero-centered.

Therefore, concurrent measurement of LD(t) and the super-localized position in PR-SMT can yield information on rotational dynamics during tracer diffusion. To detect emission from single Rh6G tracers sparsely embedded in a plasticized PVP matrix, we used a home-built PR epifluorescence microscopy setup with circularly polarized 532 nm laser excitation equipped with a CCD camera (see Fig. S2, ESI†), the details of which are described elsewhere.[48] All information on materials, sample preparation, data acquisition and subsequent PR-SMT analyses is provided in the ESI.† Pixel-by-pixel superposition of PR image sequences in a field of view (FOV) yields a movie (10 Hz) of total intensity, $I_T(t) = I_s(t) + I_p(t)$, which is utilized to obtain super-localized SM trajectories ($\{x(t),y(t)\}$). The polarization trajectories (LD(t)) were computed from $\{I_s(t),I_p(t)\}$ at each location corresponding to $\{x(t),y(t)\}$. All analyses were performed using ImageJ (NIH) and MATLAB, the algorithms for which are provided in the ESI,† along with all details of image/data analysis procedures.

3. Results

Our measurements generate sets of image sequences *via* two orthogonally polarized detection channels, as shown in Fig. 2a for a FOV containing a few Rh6G molecules in a rubbery PVP film. Fig. 2b shows pseudocolor sequential snapshots of two tracers (M1 and M2) generated *via* the quantitative superposition of the S- (red) and P- (green) polarized movies (Fig. S3, ESI†), showing changes in their positions and anisotropy. The maximum projections of these color-merged image stacks (Fig. 2c) reveal non-circular (smudged) emission owing to translational motion beyond few hundred nanometers. Further, the change in the hue (green through red) over different frames (Fig. 2b and c) allows for the identification of temporal variation in $I_s(t)$ and $I_p(t)$. Fig. 2c (right panel) shows another tracer (M3) for which super-localization of positions (Fig. 2d) reveals unambiguous translational motion. For M3, the $I_s(t)$, $I_p(t)$ and LD(t) trajectories (Fig. 2e) reveal that the LD(t) fluctuates around zero for the vast majority of the time durations, as expected from a translationally active dipole undergoing facile reorientation. While we do find that |LD(t)| is quite high (>0.2) for a couple of time points, it is necessary to first evaluate the uncertainty in LD(t) to establish rotational immobility at these instances.

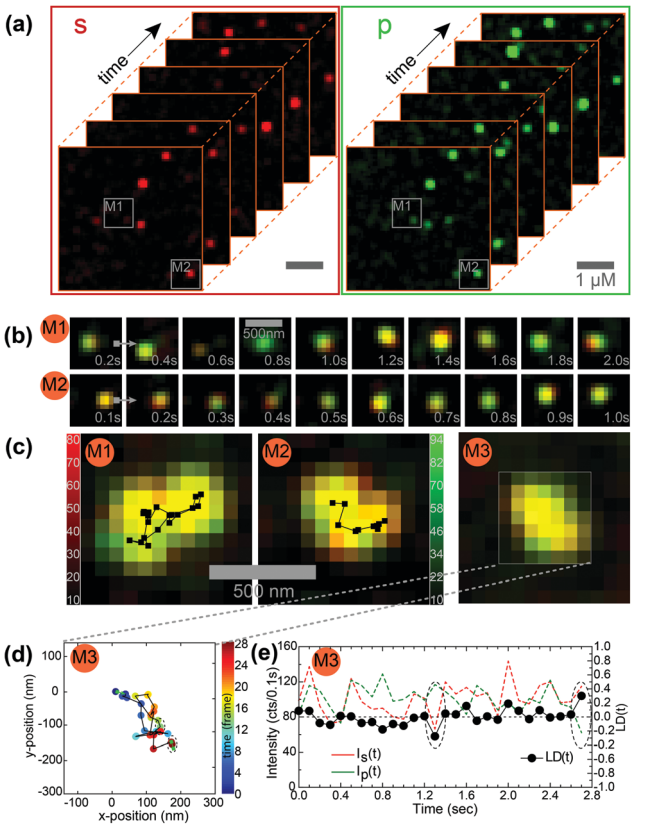

Fig. 2 (a) Sequential images of two polarised channels, denoted as red (S) and green (P), collected using the same CCD camera. (b) Pseudo-color superimposed intensity images of S- and P-channels of two SMs (M1 and M2) taken from the specified region in (a). Shade of hue represents variation of emission intensity in each channel, while change of position reflects translational motion. (c) The super-resolved trajectories of M1 and M2 overlaid with the maximum projection of pseudo-color (merged) polarization-resolved movies. (c) Left panel: Pseudo-color (merged) polarization image of an Rh6G molecule (M3); the intensity counts range from 0–75 in both red (S) and green (P) polarization channels. (d) Super-resolved trajectories showing examples of the tracer (M3) being within the LE (dashed ovals). (e) The polarised intensity and LD(t) trajectories of M3, showing high values of LD(t) at the same time frames.

We therefore collected PR movies of SMs embedded in a glassy (dehydrated) PVP matrix where the polymer network cavities are extremely compact and rigid, preventing any dipolar reorientation.[51] From the analysis of 46 immobile SM trajectories, we estimate that the standard deviation (σ) of localization is ~13 nm (Fig. S4, ESI†). As a conservative estimate, we considered

the LE to be ~40 nm ($3\sigma_{XY}$); displacement (Δq) beyond this value served as an indicator for translational movement.[52] Further, the σ of LD (σ_{LD}) for these 46 SMs was found to be ~0.1 (Fig. S4, ESI†). Based on this analysis, we infer that an event with $|LD(t)| > 0.25$ ($2.5\sigma_{LD}$) observed in PR-SMT can only be a consequence of either rotational immobility or very slow hindered reorientation of individual dipoles (for details, see ESI,† error estimation in PR-SMT).

We observe diverse dynamic characteristics for individual Rh6G tracers in the hydrated PVP matrix under an ambient RH of ~75% (Fig. 1d) owing to the lowering of the T_g to at least 40–50 K below the measurement temperature (298 K). For quantitative assessment, we classify all the tracers into three broad categories based on their translational characteristics, specifically, the radius of gyration (R_g) over their entire trajectories.[8] Although hundreds of tracers have been investigated using PR-SMT, we selected SMs with a high signal to background ratio (SBR > 3), nominal blinking and a photobleaching time of more than 3 s, which allowed for the detailed analysis of ~100 SM trajectories. Below, we use two representative SMs from each dynamic category (I, II and III) to illustrate how analysis of PR-SMT can identify genuine transient pauses during tracer navigation, while trajectories of six more SMs are provided in Fig. S5 (ESI†). PR-SMT data collected for each SM can be projected as a 3D scatter plot with localized positions and corresponding LD(t) values, as depicted in Fig. 3a–f for M4–M9. The $\{x(t),y(t)\}$ and LD(t) trajectories for these SMs are shown in Fig. 3g–l, while their distributions are provided in Fig. S6 (ESI†).

3.1 Category I – transport within localization error

The ability of PR-SMT to discriminate between immobile and mobile tracers within LE is exemplified using M4 (Fig. 3a and g) and M5 (Fig. 3b and h). Here, both tracers are apparently static with their super-localized positions well within the LE. For M4, the P(LD) is bimodal centered at ~+0.6 and ~−0.7 (Fig. 3a), which is expected of a dipole undergoing transition between two angular states. This is corroborated by the corresponding LD(t) trajectories (Fig. 3g), which reveal that the tracer remains immobile for several seconds before undergoing abrupt angular jumps to a few specific orientations. Since M4 undergoes extremely slow reorientational dynamics, it must be embedded in a compact cavity where only hindered rotation is permissible. Therefore, it is unlikely that M4 can undergo any translational motion beyond the dimensions of the cavity created by the hydrated polymer network. In contrast, M5 exhibits strikingly different reorientational dynamics. Here, P(LD(t)) is unimodal and centered around zero (Fig. 3b) suggestive of much faster (> 50 Hz) reorientational dynamics, while the LD(t) trajectories (Fig. 3h) reveal that the dipole seldom undergoes hindered rotation. Therefore, M5 may either be confined in a relatively large void of a few nanometers or may undergo localized movement between interconnected cavities within the network where translational motion is restricted to within few tens of nanometers.

3.2 Category II – transport beyond LE and within diffraction limit

In contrast to the previous situation, the SM tracers categorized in this regime exhibit translational mobility ($2R_g$) beyond the LE, such as M6 (Fig. 3c and i) and M7 (Fig. 3d and j). These two tracers undergo a net displacement of ~200 nm in (x,y), indicating unambiguous translational mobility (Fig. 3c and d). However, an inspection of position trajectories (Fig. 3i and j) reveals certain time-windows where the successive positions are very close to or within the LE. For instance, the location of M6 is seemingly invariant for the first few seconds after which there is a clear initiation of translation, while M7 exhibits translational mobility up to ~3 s, beyond which its position remains within the LE. Here, the LD(t) for the same SMs reveals new information on the translational dynamics of the tracers. While the P(LD) is centered around zero and a majority of the $|LD(t)|$ values remain well within 0.25 as expected for fast (> 50 Hz) dipolar reorientation, there are a few intermittent time points where $|LD(t)|$ is significantly high (> 0.25), such as those at 0.9 s and 1.6 s for M6 (Fig. 3i). These rotational immobility events imply that the tracer is momentarily static (translationally) at those instances. Further, we find that consecutive values of $|LD(t)|$ may exceed ~0.25 for even longer time durations, especially when successive positions are within the LE. Such a scenario is visible for M7 between 3–4.4 s where dipolar reorientation remains restricted between ~3.1–4.0 s (Fig. 3j). This implies that M7 remains translationally immobile for ~900 ms, while for the remaining time duration, it undergoes localized motion.

3.3 Category III – transport beyond diffraction limit

The SM tracers categorized in this regime undergo translational movement ($2R_g$) beyond the diffraction limit up to ~1 μm, as exhibited by M8 (Fig. 3e and k) and M9 (Fig. 3f and l). These two tracers undergo translation in slightly different environments; while M8 undergoes relatively uninhibited translation (> 500 nm), M9 is initially restricted within one region (~1 μm^2) and subsequently traverses to another confined region. For both these molecules, the scatter plots (Fig. 3e and f), as well as the position trajectories (Fig. 3k and l) depict unambiguous translation, although for a few successive time-steps, their locations remain within the LE. Here, the P(LD) is quite narrow ($\sigma_{LD} \sim 0.2$) with the mean value very close to zero, as expected for translationally active dipoles which reorient at relatively fast timescales. However, for both M8 and M9, there are a few instances where $|LD(t)|$ is greater than 0.25, which indicates that the tracers infrequently undergo intermittent pauses during navigation.

To identify momentary pauses for a translationally active tracer, it is essential to correlate displacements between consecutive frames and corresponding occurrences of hindered reorientation of each SM tracer. For instance, the vast majority of rotational hindrance (high LD(t)) events occur when successive locations are close to LE and displacements significantly more than LE are most often associated with facile dipolar reorientation ($|LD(t)| < 0.2$). This implies that the category III tracers undergo translational motion for dominant time periods and pause only for a few intermittent short time durations. In contrast, there are several time points where $|LD(t)|$ is very close to zero, but displacements at those instances are well within the LE (such as 1–2.5 s for M8 and 1–1.2 s for M9, Fig. 3k and l), suggesting that tracers undergo localized motion over these durations.

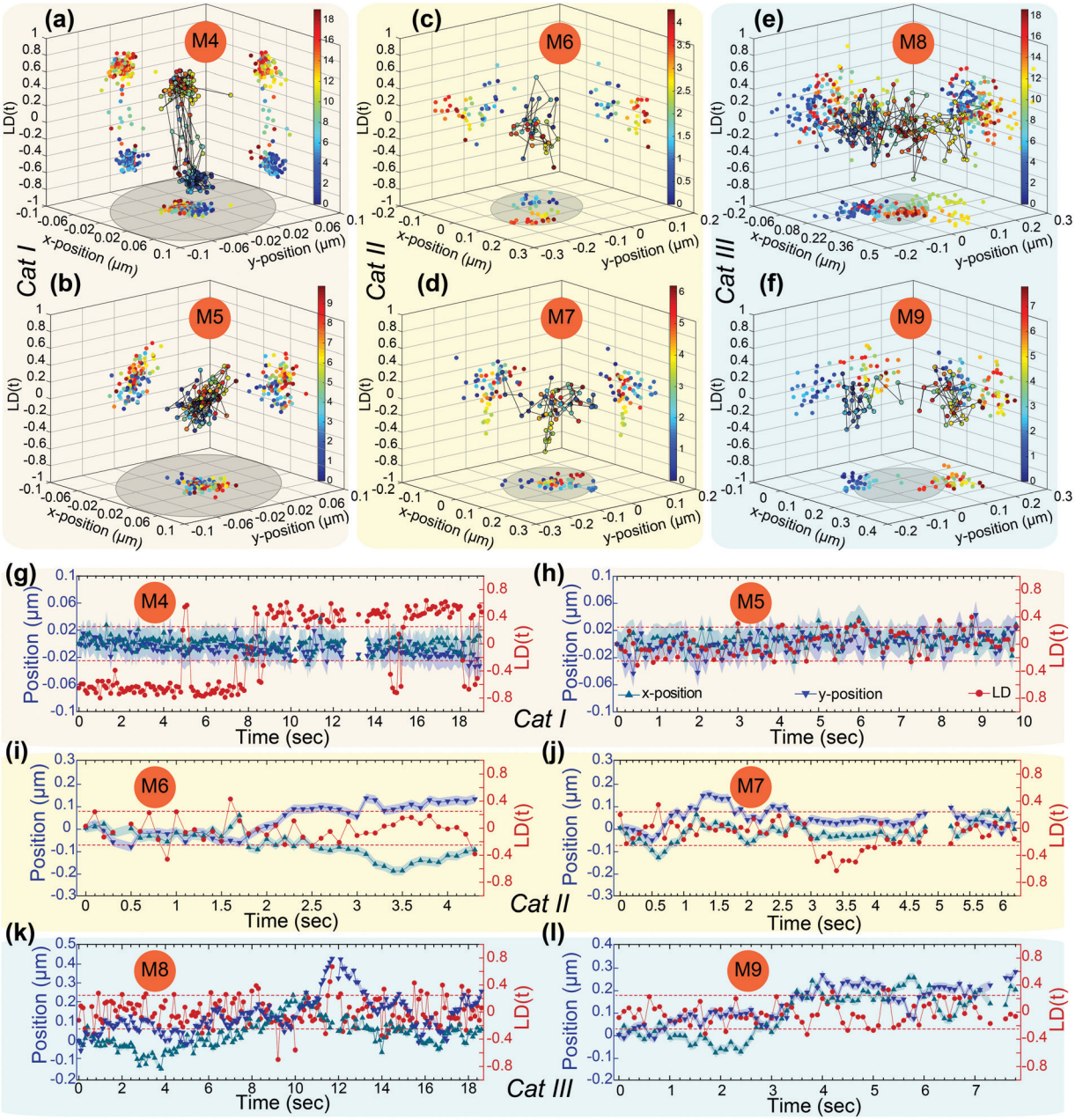

Fig. 3 Six representative single Rh6G molecules in a hydrated PVP matrix, two representatives from each of the three categories (defined in the text). (a–f) 3D scatter plots of localized $\{x(t),y(t)\}$ and LD(t) from trajectories of M4–M9. Calibration bars depict the scale of temporal evolution in seconds and grey shaded regions represent the diffraction limit. (g–l) Corresponding trajectories of super-localized $\{x(t),y(t)\}$ (filled triangles) and LD(t) (filled circles). Dashed horizontal lines represent $\pm 2.5\sigma_{LD}$. Two more SM trajectories from each motion category are provided in Fig. S5 (ESI†) and the $P(x)$, $P(y)$ and P(LD) are shown in Fig. S6 (ESI†).

3.4 Deciphering genuine im(mobility) in SM trajectories

The representative SM trajectories (Fig. 3) depict that a single tracer molecule can undergo a wide range of translational and rotational dynamics over the course of navigation, from being translationally active to being completely (rotationally and translationally) immobile. To obtain quantitative information on the occurrence of the various possibilities for individual tracers, we correlated the single-frame displacements (Δq) with the corresponding changes in LD, ($|\Delta$LD$|$), at each time-point. The details of the algorithm to perform the above correlative analysis, which enabled the assignment of diverse dynamics processes at every time-point in a PR-SMT trajectory, are provided in ESI† (Methods, Fig. S7). First, we chose events where the $\Delta q(t)$ is less than the LE and subsequently identified the time points where the tracer undergoes very slow reorientation (or only wobbles). These sets of events essentially represent authentic immobile instances in an SM trajectory. In contrast, instances of localized motion in a trajectory are characterized

by $\Delta q(t) <$ LE with facile rotation. Further, facile rotational mobility accompanied by $\Delta q(t) >$ LE are identified as translationally active events within each trajectory.

Intriguingly, we find some rare instances where displacements are beyond 40 nm while the corresponding $|LD(t)|$ is >0.25. These scenarios may arise from several contrasting possibilities. For instance, it is known that localization of a dipole in a specific orientation may result in an error of more than 40 nm.[31,33] Oriented translation of a tracer, *i.e.*, 1D movement in a nanochannel,[46,47] beyond the LE can also lead to such an observation, although it is very unlikely for an amorphous polymer film network to have such extended nanochannels. Due to this ambiguity, we refrain from considering these rare events in our trajectory analyses. We further note that Rh6G probes are isotropically oriented in the polymer matrix with equal probability in all directions (and over time). However, since we do not excite dipoles aligned along the *z*-direction (and thus, emission is not detected), momentary immobility along the *z*-direction can be misinterpreted as blinking.

We depict the outcome of our analyses on the occurrence of various dynamic scenarios during the navigation of M4–M9 in Fig. 4. We find that M4 is both translationally and rotationally immobile for the entire trajectory (Fig. 4a), while M5 undergoes localized motion for the majority of instances (Fig. 4b). It is important to note, however, that there are a few short-duration events (100–300 ms) where M5 is intermittently stuck, along with few instances (4.5 s, 8.9 s) of translation beyond the LE. For tracers which undergo movement within the diffraction limit (category II), the translational dynamics are more diverse, as exemplified by M6 and M7 (Fig. 4c and d). Both these tracers undergo clear translational motion within or beyond the LE in most instances, pausing intermittently only on a few occasions. It is interesting to note that M7 pauses for a significant time period (for $\sim$900 ms) at 3.1 s (Fig. 4d). Such instances likely signify the trapping (or association) processes of Rh6G in rigid, compact voids within the hydrated polymer network. Although the instances of displacements beyond the LE are relatively higher for category III tracers such as M8 and M9 and transient immobility is quite rare, our analysis reveals frequent occurrences of localized motion (Fig. 4e, f and Fig. S8, S9, ESI†).

3.5 PR-SMT analysis of 100 SM trajectories

To characterize the transient translational immobility of tracers, we identified the time points in each SM trajectory for which the displacements are within the LE and subsequently investigated whether dipolar reorientation is hindered or facile for these particular events. Our analysis on the identification, duration and frequency of genuine transient pauses of 100 SM tracers from categories I, II and III is presented in Fig. 5. As our objective is to probe the translationally mobile and immobile instances within LE, hereafter, we refer to these events as "mobile" and "static" or "immobile", respectively. The percent of immobile events for each trajectory is plotted in Fig. 5a against the corresponding instances where displacements, as obtained from SMT, are within the LE.

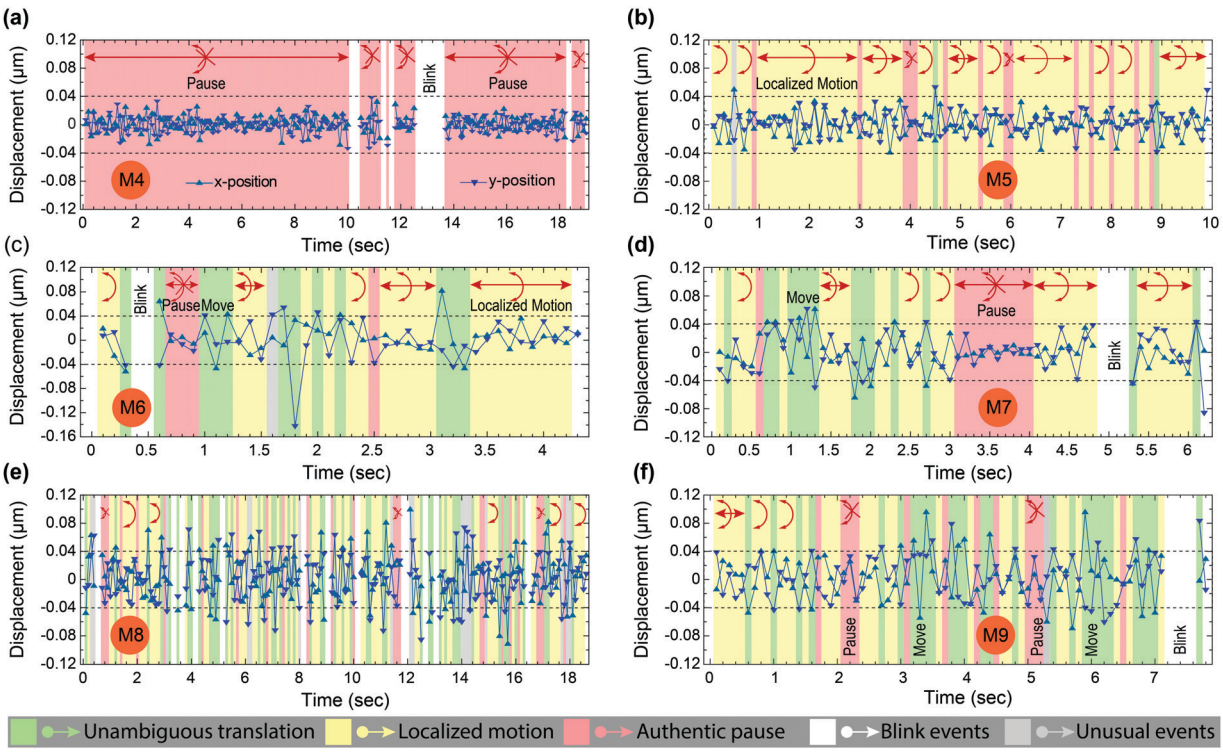

Fig. 4 (a–f) A color-coded representation of the various types of motion within each trajectory of SMs M4–M9, obtained from our PR-SMT analyses (see Fig. S7, ESI†), with data points showing the displacement at each time-point. For each SM displacement trajectory, green color indicates events of translation beyond LE, red color represents events of genuine immobility within LE, and yellow color represents events of localized motion within LE. Dashed horizontal lines represent single-frame displacements equivalent to LE.

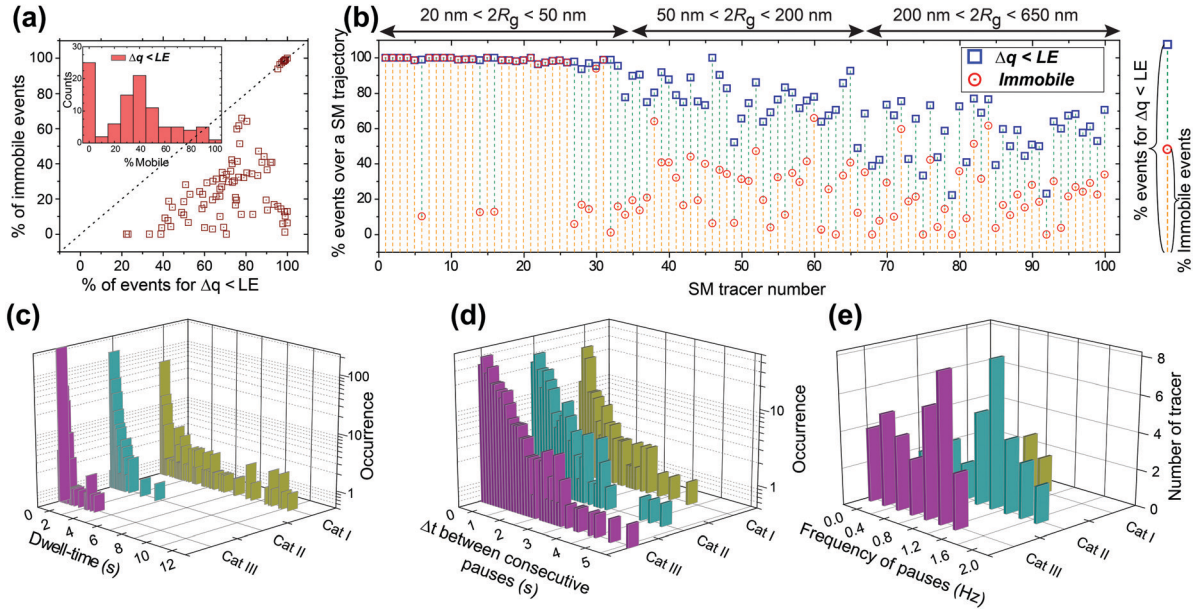

Fig. 5 PR-SMT analyses of 100 Rh6G tracers in rubbery PVP network. (a) Percent of truly immobile events extracted from PR-SMT plotted against percent of events in SMT for which displacement (Δq) are within LE. Inset shows distribution of percent of mobile events within LE, while that for immobile instances is shown in Fig. S8 (ESI†). (b) Percent of genuine immobile events within Δq < LE in each trajectory plotted against increasing R_g of the 100 SMs. The distributions of (c) pause dwell times, (d) time between consecutive pause events and (e) frequency of pauses (for individual trajectories) for each dynamic category.

We find that ~25% of the tracers lie along the diagonal, implying that super-localized positions for these trajectories indeed represent static events. However, the majority of the SMs lie below the diagonal and the extent of deviation is often pronounced, suggesting the predominance of localized motion. The distribution of the percent mobile events (Fig. 5a, inset) is found to be bimodal, with ~30% of tracers (all from Category I) being static over their entire trajectory. However, the remaining ones (from categories II and III) have diverse mobile/immobile instances during navigation, with more than 50% of tracers exhibiting localized motion for more than one-third of the trajectory length (Fig. S10, ESI†). This prompted us to investigate the fraction of locally mobile and genuinely static events in each trajectory as a function of the dynamic nature (R_g). Therefore, we plotted the percent of events in a trajectory for which displacements are LE, as well as the corresponding immobile instances (Fig. 5b), with increasing R_g for all 100 SMs. This allowed us to extract detailed information on the fraction of mobile and static events for each trajectory and further provides their relative proportions for all three dynamic categories. We find that the vast majority of category I tracers (SM1–SM34) are static for almost entire trajectory durations; however, several tracers could be identified (such as SM6, 14 and 16) which are predominantly mobile (locally) and are stuck for intermittent short durations. In contrast, our analyses reveal that the dynamics within LE for category II (SM35–SM67) and III (SM68–SM100) tracers are quite diverse (Fig. 5b). For instance, quite a few tracers (such as SM49, 61, 77 and 81) remain predominantly translationally active (*i.e.*, seldom stuck) during their course of navigation. However, some tracers, even with R_g > 50 nm (such as SM59, 72, 82 and 84), remain immobile for a considerable fraction of events when their displacements are within LE. Inspection of these trajectories reveals that such high immobile fractions are due to extremely long (>seconds) pauses rather than a high frequency of short-duration pauses (Fig. S11 and S12, ESI†).

Owing to the diverse dynamic behaviors of SMs within the hydrated polymer network, identifying the characteristic features of translational pauses requires the analysis of many tracers over their entire trajectory. Therefore, we constructed frequency histograms for dwell times (Fig. 5c), time intervals between consecutive pauses (Fig. 5d) and the frequency of immobile events (Fig. 5e) of all trajectories in each dynamic subpopulation. While the pause durations are very widely distributed for category I tracers, we find that very often their stuck events span extended durations (>s) (Fig. 5c). In contrast, category II and III tracers typically have relatively smaller dwell times (0.1–0.3 s) and progressively longer durations between consecutive stuck events (Fig. 5d). Further, for category III trajectories, the average frequency of pauses is slightly lower compared to that for category II tracers (Fig. 5e). Relatively smaller pause durations and lower frequency of pauses for tracers with the highest R_g is not surprising as these SMs have a higher tendency to undergo larger displacements (>LE).

4. Discussion

The analyses of PR-SMT trajectories reflect the extremely diverse nanoscale environments a tracer molecule encounters

during navigation in a rubbery polymer film. An intriguing outcome of our PR-SMT analysis (Fig. 5) is that the vast majority of tracers undergo intermittent translational pauses during transport through the polymer network, as evidenced from hindered or arrested reorientation. This implies that SM tracers infrequently encounter certain polymeric cavities with which they transiently associate and such a process renders the probe molecule completely immobile for ~200–500 ms. Further, quite a few tracers in various locations of the PVP film remain static for more than ~1 second. The extended durations of stasis are remarkable because hydrated PVP offers a plasticized (or rubbery) polymer network ($T_g \ll 295$ K) where segmental mobility of the polymer backbone allows rearrangement of the network, leading to the translation of small tracers embedded therein.[53] Here, it is relevant to emphasize that complete arrest of the reorientational dynamics of SM tracers is characteristic of glassy polymers, where primary (α-) relaxation processes are frozen out and secondary (β-) relaxation involving low-amplitude motion of pendant side-groups effectively restricts whole-molecule reorientation. Prior measurements on glassy PVP films have revealed that individual Rh6G molecules undergo a wobbling motion (within ~10°) far below their T_g and hindered (~0.1–1 Hz) tumbling can only be initiated near (below) the glass transition.[51] Moreover, it is well established that the timescales of SM rotational dynamics in polymer films become dramatically augmented in the vicinity of and slightly above T_g.[36,39]

Therefore, the revelation of extended pauses *via* PR-SMT suggests the existence of molecular level "glass-like" patches within the pool of the deep rubbery PVP matrix. Tracers embedded in these compact voids are unable to reorient owing to their rigidity, remaining in stasis for extended durations (~seconds) as they are unable to easily escape. Further, mobile tracers in (dominant) rubbery environments can serendipitously encounter and become entrapped in nanoscale voids, certain populations of which (inflexible cavities) render the tracers completely immobile. However, a majority of SMs eventually escape from these glassy pockets, owing to local rearrangement of the cavity, and resume transport. Such transient immobility further indicates that the rigidity of the compact polymer voids evolves slowly with time, likely as a consequence of the slow-time rearrangement of the polymer void in the immediate vicinity of the probes. While we believe that our inference is the likely scenario, it is possible that local interactions of Rh6G with PVP also contribute to our observations. Perhaps direct visualization of segmental polymer dynamics using probe-labeled PVP, similar to recent measurements on the relaxation timescales of micrometers-long entangled polymer chains,[54,55] can provide additional support to our inference.

We note that SM rotational dynamics measurements have shown that glass forming liquid (*o*-terphenyl) exists as a mosaic of spatially heterogeneous (viscoelastic) environments up to 10 K above the calorimetric T_g.[56] SM anisotropy experiments in supercooled glycerol, measured 5–23 K above the viscometric T_g (190 K), have further revealed the presence of heterogeneous fluidic pools segregated by solid-like cages (walls) which rearrange at extremely slow timescales.[40] In tune with prior observations of SM in super-cooled liquids in the vicinity of and above T_g, our results on plasticized PVP polymer suggest that remnants of glassy domains are distributed in an overwhelmingly rubbery polymer network even far above (~50 K) the T_g.

Analysis of the genuine translational pause events of the PR-SMT data further allowed us to infer the plausible spatial distribution of the molecular scale glassy pockets within the hydrated polymer network. If these are spatially segregated by microns, a SM tracer (with $R_g \sim$ 50–300 nm) would seldom encounter nanoscale glassy domains (and pause) during the course of transport. In contrast, separation of the compact cavities by a few tens of nanometers would effectively render the tracers translationally inactive due to successive association in nearby rigid domains. Our measurements reveal that for category II and III tracers, consecutive events of immobility are spaced between 0.3 and 3 s (Fig. 5d) and the frequency of transient pauses (Fig. 5e) typically varies within 0.2–1.5 Hz. This implies that during interim time periods, SM tracers are translationally active, *i.e.*, remain within the rubbery PVP network. Therefore, it is reasonable to conclude that the infrequently encountered nanoscale glassy cavities are spatially separated by several tens to a few hundreds of nanometers, surrounded by interconnected rubbery polymer. It is relevant to mention that the propensity of SM probes to escape from entrapment is very likely determined by the dynamics of the polymer chains that constitute these compact glass-like cavities. However, the factors which determine the very slow timescale dynamics of such glass-like polymeric voids remain a mystery.

5. Conclusions

To conclude, we demonstrated how dynamical information within the localization error of super-resolved trajectories can be obtained by simultaneously tracking the position and anisotropy of SM tracers. This technique is relatively simple to implement *via* the modification of existing wide-field epifluorescence microscopy setups, but a thorough analysis is necessary to identify the intricacies of the transport processes for each SM trajectory. Reaching beyond the realms of super-localization, PR-SMT allows discrimination between events of authentic pauses and localized (nano-confined) motion, thereby providing deeper insights on the heterogeneous transport of molecular tracers in complex media. Analysis of PR-SMT data for a hydrated polymer film network reveals that the transport of tracers intermittently undergoes complete arrests of translational motion, evidenced from the rotational hindrance of the probe dipole. Such infrequent events of (transient) immobility are due to fortuitous entrapment in extremely compact cavities within the polymer matrix, the rigidity of which varies very slowly with time. This implies, quite remarkably, the existence of sparsely distributed nanoscale "glassy" domains in a polymer film network far above the glass transition temperature, which are extremely challenging to detect by existing methods. We envision that PR-SMT will provide insightful information on structure and dynamics at the molecular level for a

variety of complex systems ranging from soft materials to biology and will be especially relevant to understanding the transient association phenomenon that are prevalent in heterogeneous media.

Conflicts of interest

There are no conflicts to declare.

Acknowledgements

AC acknowledges IRCC, IIT Bombay for initial funding and SERB (grant no. EMR/2017/004878) from the Department of Science and Technology (Govt. of India) for partial financial support. JM thanks IIT Bombay for PhD scholarships. Authors acknowledge Sandip Kar for help with data analyses algorithms and Mithun Chowdhury for critical inputs on the manuscript.

Notes and references

1 C. M. Anderson, G. N. Georgiou, I. E. Morrison, G. V. Stevenson and R. J. Cherry, Tracking of cell surface receptors by fluorescence digital imaging microscopy using a charge-coupled device camera, *J. Cell Sci.*, 1992, **101**, 415–425.

2 S. Wieser and G. J. Schütz, Tracking single molecules in the live cell plasma membrane—Do's and Don't's, *Methods*, 2008, **46**, 131–140.

3 S. Das, T. Yin, Q. Yang, J. Zhang, Y. I. Wu and J. Yu, Single-molecule tracking of small gtpase RAC1 uncovers spatial regulation of membrane translocation and mechanism for polarized signaling, *Proc. Natl. Acad. Sci. U. S. A.*, 2015, **112**, E267–E276.

4 M. Vrljic, S. Y. Nishimura, S. Brasselet, W. E. Moerner and H. M. McConnell, Translational diffusion of individual class II MHC membrane proteins in cells, *Biophys. J.*, 2002, **83**, 2681–2692.

5 D. Calebiro, F. Rieken, J. Wagner, T. Sungkaworn, U. Zabel, A. Borzi, E. Cocucci, A. Zürn and M. J. Lohse, Single-molecule analysis of fluorescently labeled G-protein-coupled receptors reveals complexes with distinct dynamics and organization, *Proc. Natl. Acad. Sci. U. S. A.*, 2013, **110**, 743–748.

6 F. Pinaud, S. Clarke, A. Sittner and M. Dahan, Probing cellular events, one quantum dot at a time, *Nat. Methods*, 2010, **7**, 275–285.

7 S. Habuchi, N. Satoh, T. Yamamoto, Y. Tezuka and M. Vacha, Multimode diffusion of ring polymer molecules revealed by a single-molecule study, *Angew. Chem., Int. Ed.*, 2010, **49**, 1418–1421.

8 L. C. C. Elliott, M. Barhoum, J. M. Harris and P. W. Bohn, Trajectory analysis of single molecules exhibiting non-Brownian motion, *Phys. Chem. Chem. Phys.*, 2011, **13**, 4326–4334.

9 C. H. Lee, A. J. Crosby, T. Emrick and R. C. Hayward, Characterization of heterogeneous polyacrylamide hydrogels by tracking of single quantum dots, *Macromolecules*, 2014, **47**, 741–749.

10 A. Gahlmann and W. E. Moerner, Exploring bacterial cell biology with single-molecule tracking and super-resolution imaging, *Nat. Rev. Microbiol.*, 2014, **12**, 9–22.

11 A. Kusumi, T. A. Tsunoyama, K. M. Hirosawa, R. S. Kasai and T. K. Fujiwara, Tracking single molecules at work in living cells, *Nat. Chem. Biol.*, 2014, **10**, 524–532.

12 B. Wang, J. Kuo, S. C. Bae and S. Granick, When Brownian diffusion is not Gaussian, *Nat. Mater.*, 2012, **11**, 481–485.

13 I. Bronstein, Y. Israel, E. Kepten, S. Mai, Y. Shav-Tal, E. Barkai and Y. Garini, Transient Anomalous Diffusion of Telomeres in the Nucleus of Mammalian Cells, *Phys. Rev. Lett.*, 2009, **103**, 018102.

14 S. C. Weber, A. J. Spakowitz and J. A. Theriot, Bacterial chromosomal loci move subdiffusively through a viscoelastic cytoplasm, *Phys. Rev. Lett.*, 2010, **104**, 238102.

15 G. Seisenberger, M. U. Ried, T. Endreß, H. Büning, M. Hallek and C. Bräuchle, Real-time single-molecule imaging of the infection pathway of anadeno-associated virus, *Science*, 2001, **294**, 1929–1932.

16 M. Weiss, Single-particle tracking data reveal anticorrelated fractional Brownian motion in crowded fluids, *Phys. Rev. E: Stat., Nonlinear, Soft Matter Phys.*, 2013, **88**, 010101.

17 M. J. Skaug, J. Mabry and D. K. Schwartz, Intermittent molecular hopping at the solid-liquid interface, *Phys. Rev. Lett.*, 2013, **110**, 256101.

18 S. Burov, J. H. Jeon, R. Metzler and E. Barkai, Single particle tracking in systems showing anomalous diffusion: The role of weak ergodicity breaking, *Phys. Chem. Chem. Phys.*, 2011, **13**, 1800–1812.

19 A. V. Weigel, S. Ragi, M. L. Reid, E. K. P. Chong, M. M. Tamkun and D. Krapf, Obstructed diffusion propagator analysis for single-particle tracking, *Phys. Rev. E: Stat., Nonlinear, Soft Matter Phys.*, 2012, **85**, 041924.

20 E. Barkai, Y. Garini and R. Metzler, Strange kinetics of single molecules in living cells, *Phys. Today*, 2012, **65**, 29–35.

21 A. V. Weigel, B. Simon, M. M. Tamkun and D. Krapf, Ergodic and nonergodic processes coexist in the plasma membrane as observed by single-molecule tracking, *Proc. Natl. Acad. Sci. U. S. A.*, 2011, **108**, 6438–6443.

22 J. Szymanski and M. Weiss, Elucidating the origin of anomalous diffusion in crowded fluids, *Phys. Rev. Lett.*, 2009, **103**, 038102.

23 J. Gorman, A. Chowdhury, J. A. Surtees, J. Shimada, D. R. Reichman, E. Alani and E. C. Greene, Dynamic Basis for One-Dimensional DNA Scanning by the Mismatch Repair Complex Msh2-Msh6, *Mol. Cell*, 2007, **28**, 359–370.

24 R. E. Thompson, D. R. Larson and W. W. Webb, Precise nanometer localization analysis for individual fluorescent probes, *Biophys. J.*, 2002, **82**, 2775–2783.

25 M. P. Backlund, R. Joyner and W. E. Moerner, Chromosomal locus tracking with proper accounting of static and dynamic errors, *Phys. Rev. E: Stat., Nonlinear, Soft Matter Phys.*, 2015, **91**, 062716.

26 S. C. Weber, M. A. Thompson, W. E. Moerner, A. J. Spakowitz and J. A. Theriot, Analytical tools to distinguish the effects of localization error, confinement, and medium

elasticity on the velocity autocorrelation function, *Biophys. J.*, 2012, **102**, 2443–2450.
27 M. J. Rust, M. Bates and X. Zhuang, Sub-diffraction-limit imaging by stochastic optical reconstruction microscopy (STORM), *Nat. Methods*, 2006, **3**, 793–795.
28 E. Betzig, G. H. Patterson, R. Sougrat, O. W. Lindwasser, S. Olenych, J. S. Bonifacino, M. W. Davidson, J. Lippincott-Schwartz and H. F. Hess, Imaging intracellular fluorescent proteins at nanometer resolution, *Science*, 2006, **103**, 1642–1645.
29 C. Manzo, J. A. Torreno-Pina, P. Massignan, G. J. Lapeyre, M. Lewenstein and M. F. Garcia Parajo, Weak Ergodicity Breaking of Receptor Motion in Living Cells Stemming from Random Diffusivity, *Phys. Rev. X*, 2015, **5**, 011021.
30 J. Enderlein, E. Toprak and P. R. Selvin, Polarization effect on position accuracy of fluorophore localization, *Opt. Express*, 2006, **14**, 8111–8120.
31 M. P. Backlund, A. Arbabi, P. N. Petrov, E. Arbabi, S. Saurabh, A. Faraon and W. E. Moerner, Removing orientation-induced localization biases in single-molecule microscopy using a broadband metasurface mask, *Nat. Photonics*, 2016, **10**, 459–462.
32 M. P. Backlund, M. D. Lew, A. S. Backer, S. J. Sahl and W. E. Moerner, The Role of Molecular Dipole Orientation in Single-Molecule Fluorescence Microscopy and Implications for Super-Resolution Imaging, *ChemPhysChem*, 2014, **15**, 587–599.
33 M. D. Lew, M. P. Backlund and W. E. Moerner, Rotational mobility of single molecules affects localization accuracy in super-resolution fluorescence microscopy, *Nano Lett.*, 2013, **13**, 3967–3972.
34 B. M. I. Flier, M. Baier, J. Huber, K. Müllen, S. Mecking, A. Zumbusch and D. Wöll, Single molecule fluorescence microscopy investigations on heterogeneity of translational diffusion in thin polymer films, *Phys. Chem. Chem. Phys.*, 2011, **13**, 1770–1775.
35 F. C. Hendriks, F. Meirer, A. V. Kubarev, Z. Ristanović, M. B. J. Roeffaers, E. T. C. Vogt, P. C. A. Bruijnincx and B. M. Weckhuysen, Single-molecule fluorescence microscopy reveals local diffusion coefficients in the pore network of an individual catalyst particle, *J. Am. Chem. Soc.*, 2017, **139**, 13632–13635.
36 B. M. I. Flier, M. C. Baier, J. Huber, K. Müllen, S. Mecking, A. Zumbusch and D. Wöll, Heterogeneous diffusion in thin polymer films as observed by high-temperature single-molecule fluorescence microscopy, *J. Am. Chem. Soc.*, 2012, **134**, 480–488.
37 J. R. Lakowicz, *Principles of Fluorescence Spectroscopy*, Springer US, Boston, MA, 2006.
38 M. Dorfschmid, K. Müllen, A. Zumbusch and D. Wöll, Translational and Rotational Diffusion during Radical Bulk Polymerization: A Comparative Investigation by Full Correlation Fluorescence Correlation Spectroscopy (fcFCS), *Macromolecules*, 2010, **43**, 6174–6179.
39 A. Schob, F. Cichos, J. Schuster and C. Von Borczyskowski, Reorientation and translation of individual dye molecules in a polymer matrix, *Eur. Polym. J.*, 2004, **40**, 1019–1026.
40 R. Zondervan, F. Kulzer, G. C. G. Berkhout and M. Orrit, Local viscosity of supercooled glycerol near Tg probed by rotational diffusion of ensembles and single dye molecules, *Proc. Natl. Acad. Sci. U. S. A.*, 2007, **104**, 12628–12633.
41 A. G. T. Ruiter, J. A. Veerman, M. F. Garcia-Parajo and N. F. Van Hulst, Single molecule rotational and translational diffusion observed by near-field scanning optical microscopy, *J. Phys. Chem. A*, 1997, **101**, 7318–7323.
42 E. Mei, J. Tang, J. M. Vanderkooi and R. M. Hochstrasser, Motions of single molecules and proteins in trehalose glass, *J. Am. Chem. Soc.*, 2003, **125**, 2730–2735.
43 T. Ha, J. Glass, T. Enderle, D. S. Chemla and S. Weiss, Hindered Rotational Diffusion and Rotational Jumps of Single Molecules, *Phys. Rev. Lett.*, 1998, **80**, 2093–2096.
44 J. N. Forkey, M. E. Quinlan, M. A. Shaw, J. E. T. Corrie and Y. E. Goldman, Three-dimensional structural dynamics of myosin V by single-molecule fluorescence polarization, *Nature*, 2003, **422**, 399–404.
45 S. A. Rosenberg, M. E. Quinlan, J. N. Forkey and Y. E. Goldman, Rotational Motions of Macro-molecules by Single-Molecule Fluorescence Microscopy, *Acc. Chem. Res.*, 2005, **38**, 583–593.
46 R. Pramanik, T. Ito and D. A. Higgins, Single molecule wobbling in cylindrical mesopores, *J. Phys. Chem. C*, 2013, **117**, 3668–3673.
47 R. Pramanik, T. Ito and D. A. Higgins, Molecular length dependence of single molecule wobbling within surfactant- and solvent-filled silica mesopores, *J. Phys. Chem. C*, 2013, **117**, 15438–15446.
48 S. Bhattacharya, D. K. Sharma, S. Saurabh, S. De, A. Sain, A. Nandi and A. Chowdhury, Plasticization of poly(vinylpyrrolidone) thin films under ambient humidity: Insight from single-molecule tracer diffusion dynamics, *J. Phys. Chem. B*, 2013, **117**, 7771–7782.
49 H. Sosa, E. J. G. Peterman, W. E. Moerner and L. S. B. Goldstein, ADP-induced rocking of the kinesin motor domain revealed by single-molecule fluorescence polarization microscopy, *Nat. Struct. Biol.*, 2001, **8**, 540–544.
50 G. J. Schütz, H. Schindler and T. Schmidt, Imaging single-molecule dichroism, *Opt. Lett.*, 1997, **22**, 651.
51 S. Bhattacharya, D. K. Sharma, S. De, J. Mahato and A. Chowdhury, Heterogeneity during Plasticization of Poly(vinylpyrrolidone): Insights from Reorientational Mobility of Single Fluorescent Probes, *J. Phys. Chem. B*, 2016, **120**, 12404–12415.
52 X. Michalet, Mean square displacement analysis of single-particle trajectories with localization error: Brownian motion in an isotropic medium, *Phys. Rev. E: Stat., Nonlinear, Soft Matter Phys.*, 2010, **82**, 041914.
53 E. Braeken, G. De Cremer, P. Marsal, G. Pèpe, K. Müllen and R. A. L. Vallée, Single Molecule Probing of the Local Segmental Relaxation Dynamics in Polymer above the Glass Transition Temperature, *J. Am. Chem. Soc.*, 2009, **131**, 12201–12210.
54 M. Keshavarz, H. Engelkamp, J. Xu, E. Braeken, M. B. J. Otten, H. Uji-I, E. Schwartz, M. Koepf, A. Vananroye, J. Vermant, R. J. M. Nolte, F. De Schryver, J. C. Maan, J. Hofkens, P. C. M. Christianen and A. E. Rowan, Nanoscale study of polymer dynamics, *ACS Nano*, 2016, **10**, 1434–1441.
55 M. Abadi, M. F. Serag and S. Habuchi, Entangled polymer dynamics beyond reptation, *Nat. Commun.*, 2018, **9**, 5098.
56 L. A. Deschenes and D. A. Vanden Bout, Heterogeneous dynamics and domains in supercooled o-terphenyl: A single molecule study, *J. Phys. Chem. B*, 2002, **106**, 11438–11445.

